

Crossed real nodal-line phonons in gold monobromide

Yilin Han,¹ Yichen Liu,¹ Chaoxi Cui,¹ Cheng-Cheng Liu,^{1,*} and Zhi-Ming Yu^{1,†}

¹*Key Lab of advanced optoelectronic quantum architecture and measurement (MOE),
Beijing Key Lab of Nanophotonics & Ultrafine Optoelectronic Systems,
and School of Physics, Beijing Institute of Technology, Beijing 100081, China*

Spacetime inversion symmetry can generate intriguing types of spinless excitations in crystalline materials. Here, we propose a topological phase protected by spacetime inversion symmetry—the crossed real nodal line (RNL) in the phonon spectrum of gold monobromide (AuBr). In AuBr, there exist four straight nodal lines, which are linked by a crossed nodal line formed by two lower bands. Remarkably, each adjacent two of the four straight nodal lines is a pair, forming a crossed RNL with nontrivial real Chern number. Such configuration and pairing mode of RNL have never been reported. The crossed RNL exhibits unique surface and hinge states distinguished from that of the conventional RNLs. The symmetry protection and the transformation under the symmetry-preserving strain of the crossed RNL are also investigated. Our results open the door to a new class of topological states, and predict its realization in experimentally synthesized material.

I. INTRODUCTION

The crystalline materials can exhibit various excitations around band degeneracies in their energy spectrums, such as electronic and phonon band structure [1–11]. The most common degeneracy is the nodal point [12–23], which has zero-dimensional (0D) manifold, and widely appears in 1D, 2D and 3D systems. With additional symmetries, the degeneracy with 1D manifold can appear, leading to the topological nodal-line phases [24–32].

Generally, the nodal line occurs in a mirror plane formed by two bands with opposite mirror eigenvalues [24, 30]. Since the mirror can quantize the Berry phase into 0 and π , the mirror nodal line hosts a Z_2 topological charge, and is topologically protected by π Berry phase [33, 34]. In addition, the nodal line can widely exist in the spinless systems with spacetime inversion symmetry (\mathcal{PT}), where the Berry phase also is quantized [35, 36]. Interestingly, the \mathcal{PT} symmetry can protect another Z_2 topological quantity, known as second Stiefel-Whitney number w_2 or the real Chern number ν_R [37–43]. Therefore, the nodal line in \mathcal{PT} -symmetric spinless systems can be classified as the conventional one that is solely protected by π Berry phase, and the real nodal line (RNL) that is protected by both π Berry phase and the real Chern number ν_R .

The RNL, distinguished from the conventional nodal line, is not alone but must be linked by an additional nodal line formed by lower bands [38, 40]. The linked structure is a typical characteristic of the RNL. Besides, the RNL must occur in pairs, due to the nontrivial real Chern number [41]. The argument is similar to that of a Weyl point with finite Chern number [12, 44]. Consider a 2D slice in the Brillouin zone (BZ) of a 3D \mathcal{PT} -symmetric spinless system. The real Chern number of this slice is

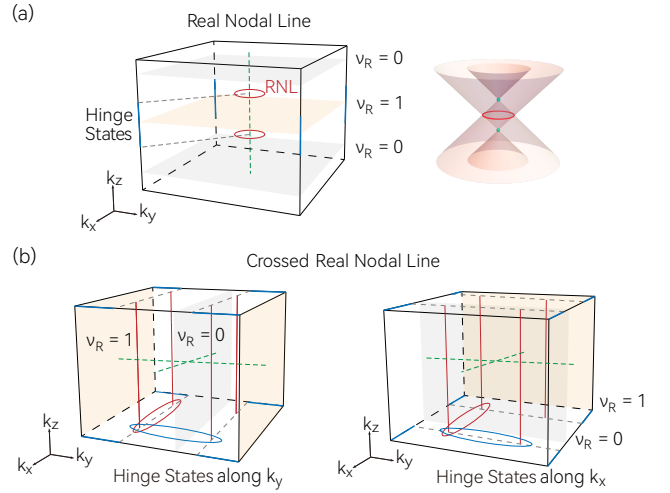


FIG. 1. Schematic figures showing two types of RNL configuration. (a) Conventional RNL configuration, where the pair of real nodal loops formed by two middle bands (red circle) are linked by another nodal line formed by two bottom bands (green dotted lines), with its band structures shown in the right. (b) Crossed RNL proposed in this work. All the four straight nodal lines (red lines) are conventional nodal line featuring nontrivial π Berry phase. However, they are linked by a crossed nodal line (green dotted line), and each adjacent two of the four straight nodal lines *together* (wrapped by blue and red circles) form a RNL with trivial Berry phase but nontrivial real Chern number ν_R . Thus, the systems with crossed RNL can exhibit hinge states in both k_x and k_y directions. In contrast, the conventional RNL state has hinge states in only one direction.

changed by one when it moves across a RNL. Since the BZ is periodic, the slice must cross another RNL to make sure that its real Chern number is not changed when it return to its original position. Since the real Chern insulator is a second-order topological insulator [45–59] hosting a corner state, this argument also indicates the appearance of the hinge states connecting two RNLs in the topological RNL systems [43].

* ccliu@bit.edu.cn

† zhiming-yu@bit.edu.cn

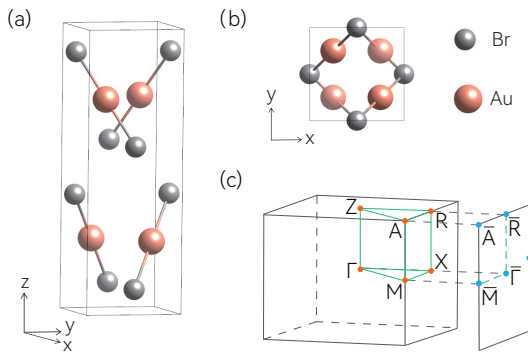


FIG. 2. (a) Side view and (b) top view of the crystal structure for 3D AuBr. (c) The bulk BZ and the (010) surface BZ for AuBr.

The material candidate of RNL is firstly proposed by Anh *et al.* in Ref. [38]. Subsequently, the RNL is predicted to exist in a few electronic systems with negligible spin-orbit coupling [43, 60], and artificial periodic systems [61–64]. Moreover, some theoretical works have constructed suitable model to study the RNL [65–68]. However, the RNL in all current studies has the same configuration that is illustrated in Fig. 1(a). The RNL occurs when four bands successively intersect, and it is the loop formed by the two middle bands and is linked by another nodal lines formed by the two bottom (top) bands [see Fig. 1(a)]. For the conventional RNL state, it generally has hinge states in only one direction, as shown in Fig. 1(a).

In this work, we propose a type of RNL that is different from the conventional RNL, and predict its realization in the phonon spectrum of experimentally synthesized 3D materials AuBr. We show that there are four straight nodal lines passing through the entire BZ in the phonon spectrum of AuBr. While the four straight lines are conventional nodal lines, each adjacent two of them is paired to form a RNL, possessing nontrivial $\nu_R = 1$. A typical feature of the RNL is the linking structure. For the RNL in AuBr, we find that the four straight nodal lines indeed are linked by a crossed nodal line formed by lower bands. Thus, we term such nodal lines as crossed RNL, and its configuration is illustrated in Fig. 1(b). For crossed RNL, we have a pair of RNLs in two directions, say, k_x and k_y directions [see Fig. 1(b)]. Consequently, the crossed RNL can have hinge states in both k_x and k_y directions. This is completely different from the conventional RNL. Moreover, the surface state of AuBr also is different from that in previously reported RNL materials. Furthermore, we find that the crossed RNL has unique evolutionary behavior under symmetry-preserving strain, namely, it disappears when the strain is within a certain range, but *reappears* by further increasing the strain.

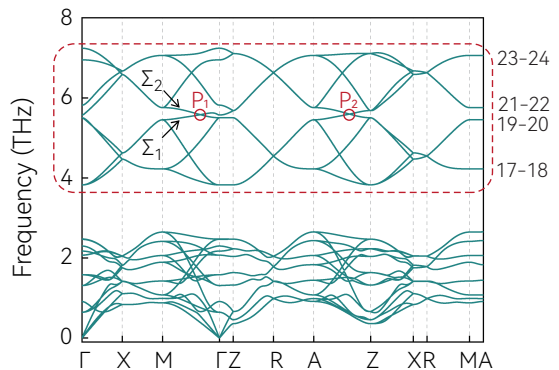


FIG. 3. Calculated phonon spectrum of 3D AuBr. The group of bands from 17th to 24th are our focus (circled by red). Here, two band crossing points P_1 and P_2 on paths ΓM and AZ are marked in red, which belong to the four straight nodal lines passing through the entire BZ. Phonon bands along ZR path are doubly degenerate, forming a crossed nodal line, due to the C_{4z} in 3D AuBr.

II. PHONON SPECTRUM AND CROSSED RNL

The 3D AuBr has been experimentally synthesized in 1978 [69, 70]. The crystalline structure of AuBr is plotted in Figs. 2(a-b), from which one observes that there are four Au and four Br atoms in a unit cell. The AuBr has a tetragonal lattice and belongs to the space group No. 138 ($P4_2/nm$). From our first-principles calculation, the relaxed lattice constants for AuBr are $a = b = 4.21 \text{ \AA}$ and $c = 12.30 \text{ \AA}$. The bulk BZ and (010) surface BZ of AuBr are illustrated in Fig. 2(c). The symmetry operators belonging to AuBr and relevant here are spatial inversion (\mathcal{P}), four-fold rotation (C_{4z}), several mirrors (M_z , M_x , M_y , M_{110} , and $M_{\bar{1}\bar{1}0}$), and time-reversal symmetry (\mathcal{T}).

The phonon spectrum of AuBr along high-symmetry paths is plotted in Fig. 3, from which one notes that there are a group of bands (17th-24th phonon bands) that is well separated from others in frequency. We first investigate the two band crossing points on paths ΓM and AZ formed by the two middle bands (20th and 21th bands) of this group of bands, which are labeled as P_1 and P_2 [see Fig. 3]. Since the AuBr has both \mathcal{P} and \mathcal{T} , P_1 (P_2) can not be isolated but a point on a nodal line [24]. As discussed by Zhang *et al.* [71], the position of the nodal line can be determined by calculating the representations of the bands forming the point. Here, we calculate the band representations of the 20th and 21th bands on path ΓM to determine the position of the nodal

TABLE I. Part of the character table of point group C_{2v} . Only two irreducible representations are presented.

| C_{2v} | E | $C_{2,110}$ | M_z | M_{110} |
|------------|-----|-------------|-------|-----------|
| Σ_1 | 1 | 1 | 1 | 1 |
| Σ_2 | 1 | -1 | 1 | -1 |

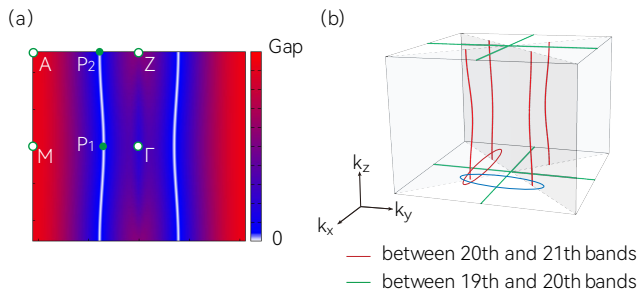


FIG. 4. Schematic figure showing the location of the nodal lines (a) in the k_{110} plane, and (b) in the BZ, formed by two middle bands (20th and 21th bands). Each adjacent two of the four straight nodal lines in (b) can be paired to form a RNL with nontrivial $\nu_R = 1$, connected by the crossed nodal lines formed by 19th and 20th bands along the ZR path (green lines).

line including P_1 . For path ΓM , its litter point group is C_{2v} , indicating that path ΓM has two mirrors: M_z and M_{110} . The band representations of the two relevant bands are respectively obtained as Σ_1 and Σ_2 , as shown in Fig. 3. From the character table of C_{2v} (see Table I), we find that Σ_1 and Σ_2 have same eigenvalues for M_z but opposite eigenvalues for M_{110} . This means that the nodal line containing P_1 point may be within the M_{110} plane, which also can be inferred from the effective Hamiltonian of the P_1 point [5]. By a careful scanning on the k_{110} plane, we find that there indeed exist a nodal line passing through the entire BZ, which includes both P_1 and P_2 points, as shown in Fig. 4(a). Due to the C_{4z} symmetry, there are four such nodal lines in total in the BZ [see Fig. 4(b)].

The four straight nodal lines in k_{110} ($k_{\bar{1}10}$) plane are conventional nodal lines protected by both M_{110} ($M_{\bar{1}10}$) and \mathcal{PT} symmetries, and hosting nontrivial π phase. However, below the four nodal lines, the phonon bands along the ZR path also are doubly degenerate [see Fig. 3]. The configuration of the four straight nodal lines and the nodal lines along ZR path are plotted in Fig. 4(b), which is reminiscent of the linking structure of the RNL if we take each adjacent two of the four straight nodal lines as a pair [see Fig. 4(b)]. To directly demonstrate the real topology of the paired straight nodal lines, we calculate the Wilson loops at two slices that are separated by them for the four bands from 17th to 20th. Here, we consider the two slices at $k_y = 0$ and $k_y = \pi$ planes.

The calculated Wilson loops are presented in Fig. 5, from which one notices that for $k_y = 0$ and $k_y = \pi$ planes, there are even (zero) and odd (one) crossing points at π axis, respectively. This indicates that the $k_y = 0$ ($k_y = \pi$) plane is trivial (nontrivial) with real Chern number $\nu_R = 0$ ($\nu_R = 1$). The difference of the ν_R of $k_y = 0$ and $k_y = \pi$ planes directly shows the two straight nodal lines at $0 < k_y < \pi$ region as a whole is a RNL with $\nu_R = 1$. Again, the C_{4z} symmetry guarantees the other three pairs of the straight nodal lines also are RNLs.

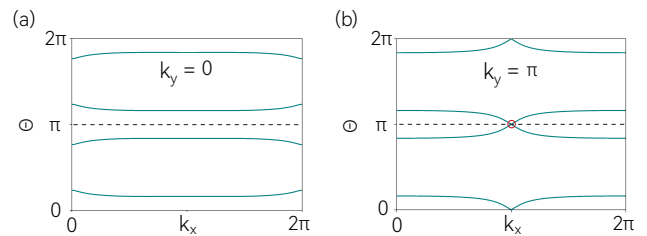


FIG. 5. (a) The Wilson loop of the 17th to 20th bands calculated in the $k_y = 0$ plane and (b) $k_y = \pi$ plane along the k_z direction. The zero (even) and one (odd) crossing point at $\theta = \pi$ indicates the planes $k_y = 0$ and $k_y = \pi$ having trivial and nontrivial real Chern number, respectively.

Since the RNL constructed by the straight nodal lines are linked by the crossed nodal lines along the two inequivalent ZR paths, we term it as crossed RNL. Apparently, the crossed RNL phase in AuBr is completely different from that in ABC-stacked graphdiyne, and show distinguished properties as discussed below.

III. TOPOLOGICAL SURFACE AND HINGE STATES

A. Topological surface state

For (010) and (100) surfaces which are connected by C_{4z} , they should have even surface states in the gap between 20th and 21th bands, as there are always two straight nodal lines that are projected into the same position of the corresponding surface BZ. This is confirmed by our calculations on the surface local density of states on (010) surface, as shown in Fig. 6, where two surface states connecting the straight nodal lines can be clearly observed.

Interestingly, the two surface states are degenerate at $\bar{R}\bar{A}$ path with $k_z = \pi$ [see Fig. 6(b)]. A generic point in the $\bar{R}\bar{A}$ path of the (010) surface has a combined sym-

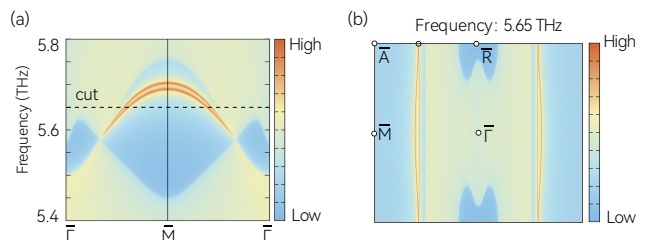


FIG. 6. (a) The surface local density of states of the phonons on the (010) surface along path $\bar{\Gamma}-\bar{M}-\bar{\Gamma}$. (b) The isofrequency arcs cut at 5.65 THz.

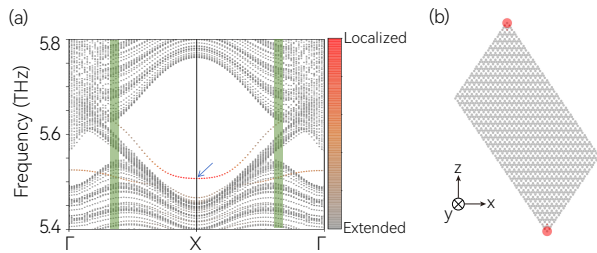


FIG. 7. (a) Spectrum for a tubelike geometry sample. The crossed RNL is located in the green shaded area. A doubly degenerate topological hinge state connecting the two crossed RNLs can be clearly observed. (b) The charge density distribution of the hinge state at X point [marked by blue arrow in (a)] in real space.

metry $G_x\mathcal{T}$ with $G_x = \{M_x|00\frac{1}{2}\}$. Since

$$\begin{aligned} (G_x\mathcal{T})^2 &= \mathcal{T}^2\{M_x|00\frac{1}{2}\}\{M_x|00\frac{1}{2}\} \\ &= \{E|001\}, \end{aligned} \quad (1)$$

with E the identity operator, one has

$$(G_x\mathcal{T})^2 = -1, \quad (2)$$

for $k_z = \pi$ line, i.e. $\bar{R}\bar{A}$ path. Thus, all the bands at $\bar{R}\bar{A}$ path are at least doubly degenerate, due to the Kramers-like degeneracy.

B. Topological hinge state

Since the AuBr has crossed RNL in its phonon spectrum, one can expect that in addition to the 2D surface states, the AuBr also should have topologically protected 1D hinge states.

The position of the hinge state can be inferred from the Z_2 invariant ν_R for the 2D slice in bulk BZ. As aforementioned, the $k_y = \pi$ plane is nontrivial with $\nu_R = 1$ [see Fig. 5(b)]. Then, all the planes within $k_y \in [-\pi, -k_c)$ and $k_y \in (k_c, \pi]$ ($k_c \simeq 0.38\pi$) would have $\nu_R = 1$, as the 20th and 21th phonon bands are gapped in this region. Similarly, the planes within $k_y \in (-k_d, k_d)$ ($k_d \simeq 0.33\pi$) would have $\nu_R = 0$. The interval of $k_y \in (k_d, k_c)$ is the location of the crossed RNL. The slices with $\nu_R = 1$ are 2D real Chern insulators and then must exhibit at least a pair of \mathcal{PT} connected corner states. All these corner states constitute the hinge state of the AuBr. To explicitly demonstrate it, we calculate the spectrum of the AuBr with a tubelike geometry shown in Fig. 7(b), which is finite in the x - z plane but periodic in the y direction. The result is plotted in Fig. 7(a), where the color denotes the degree of locality of the bands. One observes that a pair of localized states exist in the interval $k_y \in [-\pi, -k_c)$ and $k_y \in (k_c, \pi]$ and disappear when $k_y \in (-k_d, k_d)$. By further checking the spatial distribution for these state at X point ($k_y = \pi$), we find they are exactly corner states

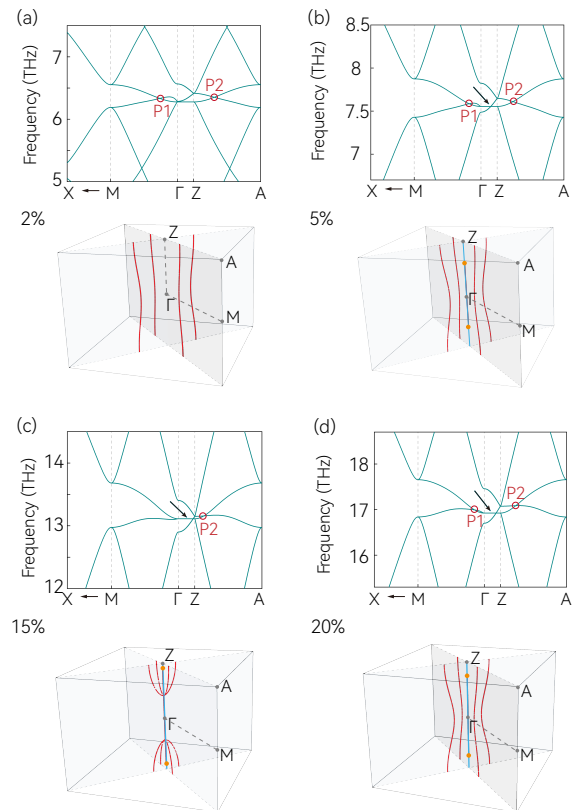


FIG. 8. The phonon spectrums along path X-M- Γ -Z-A and the shape of RNLs in k -space under the (a) 2%, (b) 5%, (c) 15%, and (d) 20% compressive stress, respectively. Here, the blue lines represent the nodal line formed by the two-degenerated bands on path ΓZ , and the orange dot represents the triple-degenerated point formed on path ΓZ .

[see Fig. 7(b)]. These corner states constitute the hinge state of the AuBr [see Fig. 7(a)].

In contrast to all the previous RNL states, in which the hinge state only appears in one direction, the crossed RNL in AuBr can feature hinge states in two directions. As shown in Fig. 4(b), the two straight nodal lines circled in blue in k_x direction also form a RNL. From C_{4z} symmetry in AuBr, one easily knows that all the planes within $k_x \in [-\pi, -k_c)$ and $k_x \in (k_c, \pi]$ ($k_c \simeq 0.38\pi$) also are 2D real Chern insulators with $\nu_R = 1$. Thus, for the AuBr with a similar tubelike geometry [see Fig. 7(b)] but being periodic in x direction, it also should exhibit a hinge state that is similar to the hinge state in Fig 7, and then is not explicitly shown here.

IV. TRANSFORMATION OF THE CROSSED RNL UNDER STAIN

Finally, we study the transformation of the crossed RNL in AuBr under symmetry-persevering strain. Since the pair of the crossed RNLs are well separated in momentum space, they are robust against the small per-

turbations. By applying a compressive stress, the four inequivalent P_1 points at $k_z = 0$ plane will move toward Γ point, making the four straight nodal line distorted [see Fig. 8(a) and 8(b)]. However, each adjacent two of the four nodal lines still form a crossed RNL. When the critical stress is of 2%, the gap at point Γ between the two middle bands (20th and 21th bands) closes [see Fig. 8(a)], and a band inversion occurs as increasing compressive stress, resulting in a nodal line formed by 20th and 21th bands and a triply degenerate point [72–74] on path ΓZ [see Fig. 8(b)]. Keep increasing the stress, the four inequivalent P_1 points continue to move toward Γ point and merge into the nodal line on ΓZ path. Meanwhile, the four nodal lines become a crossed nodal loop, as shown in Fig. 8(c). As the stress keeping increase, the crossed nodal loop shrinks but will not disappear. This is because the P_2 point at AZ path is a movable but unremovable point, as demonstrated by Li et. al. [75]. Thus, the crossed nodal loop will expand again when the stress continues to increase. Remarkably, the crossed RNLs reappear around the 20% compressive stress as shown in Fig. 8(d) and Fig. 9(b).

V. DISCUSSIONS

In this work, we propose the concept of crossed RNL and predict its realization in the phonon spectrum of 3D AuBr. The configuration of the crossed RNL is completely different from the previously reported RNL. Similar to the conventional RNL, We show that the crossed RNL also exhibit two topological invariants: π Berry phase and real Chern number, then possessing both topological surface states and hinge states. However, the topological boundary state in 3D AuBr is distinguished from that of the conventional RNL. Moreover, the crossed RNL in AuBr is robust against the symmetry-persevering perturbations and show unique transformation under uniform strain.

Besides phonon spectrum, the crossed RNL also can appear in the electronics bands of the materials with negligible spin-orbit coupling. Moreover, the artificial systems such as acoustic and photonic crystals may be promising platforms for realizing the crossed RNL, due to the highly flexible in tuning hopping parameters [76–82].

ACKNOWLEDGMENTS

The authors thank Si Li and J. Xun for helpful discussions. This work is supported by the National Key R&D Program of China (Grant No. 2020YFA0308800), the Science Fund for Creative Research Groups of NSFC (Grant No. 12321004), and the National Science Foundation of China (Grant Nos. 12234003 and 12004035). Yilin Han and Yichen Liu contributed equally to this work.

Appendix A: Calculation Method

The first-principles calculation of 3D AuBr were conducted via the Vienna ab initio simulation package (VASP) [83, 84]. The projector augmented wave (PAW) pseudopotentials [85, 86] were adopted in the calculation and generalized gradient approximation (GGA) [87] of the Perdew-Burke-Ernzerhof (PBE) functional [88] was selected as the exchange correlation potential. The 2D Brillouin zone (BZ) was sampled using Monkhorst-Pack k-mesh [89] with a size of $11 \times 11 \times 4$. The energy cutoff was set to 600 eV and the energy convergence criteria was 10^{-8} eV. The phonon band structures of AuBr was calculated by the PHONOPY package [90]. Furthermore, based on the first-principles calculation, the Wannier tight-binding (TB) model for the low-energy bands of 3D AuBr was constructed by Wannier90 [91, 92] for the subsequent higher-order band topology calculation. The surface states and the scanning of the crossed RNL are both displayed via Wanniertools [93].

The electronic band structure of AuBr with and without spin-orbit coupling (SOC) is calculated via NANOD-CAL package [94].

Appendix B: The Wilson loop of the Crossed RNL with and without compressive strain

As discussed in the main text, the switch in topology with k_y from $\nu_R = 0$ to $\nu_R = 1$ dictates the existence of crossed RNL between the two planes. It also follows that each RNL carries this nontrivial 2D topological charge $\nu_R = 1$ defined on a 2D torus surrounding the RNL, as shown in Fig. 9. Figures 9(a) and 9(b) show the calculated the Wilson loop on the 2D torus of the 3D AuBr without strain and with 20% compression stress, respectively. The odd (one) crossing point at $\theta = \pi$ in

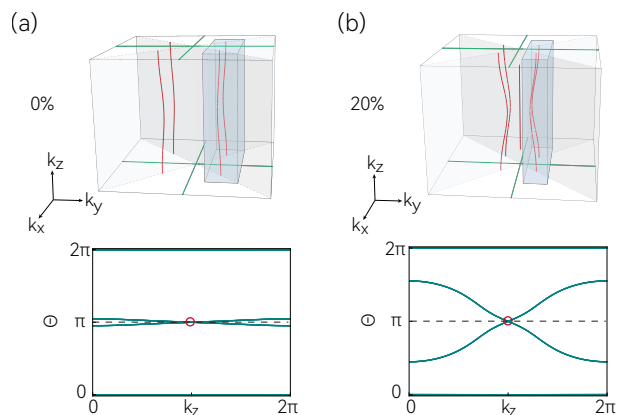


FIG. 9. Wilson loop of the 17th to 20th bands calculated on a 2D torus (marked as blue), which includes a pair of straight nodal line. (a) shows the Wilson loop for the 3D AuBr without strain and (b) shows that with 20% compressive stress.

Fig. 9 demonstrate that the crossed RNL exists in both cases.

Appendix C: Electronic band structure of AuBr

In addition to the phonon spectrum, the crossed RNL could theoretically also appear in the electronic bands of the AuBr without SOC, as the two spectrum respect the symmetry of $\mathcal{PT}^2 = 1$. Here, we calculate the electron bands of 3D AuBr without and with SOC [see Fig. 10(a) and (b)]. However, the bands are relatively messy and no obvious RNL band structure is found near the Fermi level.

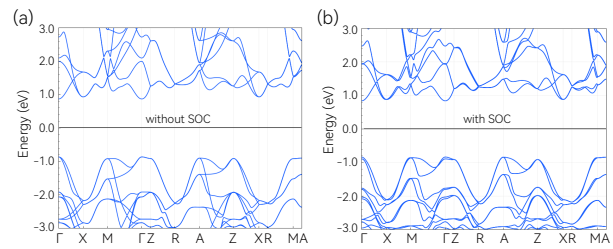


FIG. 10. Band structure of the 3D AuBr (a) without SOC and (b) with SOC.

-
- [1] N. P. Armitage, E. J. Mele, and A. Vishwanath, Weyl and Dirac semimetals in three-dimensional solids, *Reviews of Modern Physics* **90**, 015001 (2018).
- [2] B. Bradlyn, J. Cano, Z. Wang, M. G. Vergniory, C. Felser, R. J. Cava, and B. A. Bernevig, Beyond dirac and weyl fermions: Unconventional quasiparticles in conventional crystals, *Science* **353**, aaf5037 (2016).
- [3] B. Q. Lv, T. Qian, and H. Ding, Experimental perspective on three-dimensional topological semimetals, *Reviews of Modern Physics* **93**, 025002 (2021).
- [4] A. Bouhon, Q. Wu, R.-J. Slager, H. Weng, O. V. Yazyev, and T. Bzdušek, Non-Abelian reciprocal braiding of Weyl points and its manifestation in ZrTe, *Nature Physics* **16**, 1137 (2020).
- [5] Z.-M. Yu, Z. Zhang, G.-B. Liu, W. Wu, X.-P. Li, R.-W. Zhang, S. A. Yang, and Y. Yao, Encyclopedia of emergent particles in three-dimensional crystals, *Science Bulletin* **67**, 375 (2022).
- [6] Z. Zhang, G.-B. Liu, Z.-M. Yu, S. A. Yang, and Y. Yao, Encyclopedia of emergent particles in type-IV magnetic space groups, *Physical Review B* **105**, 104426 (2022).
- [7] Z. Zhang, W. Wu, G.-B. Liu, Z.-M. Yu, S. A. Yang, and Y. Yao, Encyclopedia of emergent particles in 528 magnetic layer groups and 394 magnetic rod groups, *Physical Review B* **107**, 075405 (2023).
- [8] T. Zhang, Z. Song, A. Alexandradinata, H. Weng, C. Fang, L. Lu, and Z. Fang, Double-Weyl Phonons in Transition-Metal Monosilicides, *Physical Review Letters* **120**, 016401 (2018).
- [9] B. W. Xia, R. Wang, Z. J. Chen, Y. J. Zhao, and H. Xu, Symmetry-Protected Ideal Type-II Weyl Phonons in CdTe, *Physical Review Letters* **123**, 065501 (2019).
- [10] J. Zhu, W. Wu, J. Zhao, C. Chen, Q. Wang, X.-L. Sheng, L. Zhang, Y. X. Zhao, and S. A. Yang, Phononic real Chern insulator with protected corner modes in graphynes, *Physical Review B* **105**, 085123 (2022).
- [11] R. Wang, B. W. Xia, Z. J. Chen, B. B. Zheng, Y. J. Zhao, and H. Xu, Symmetry-protected topological triangular weyl complex, *Phys. Rev. Lett.* **124**, 105303 (2020).
- [12] X. Wan, A. M. Turner, A. Vishwanath, and S. Y. Savrasov, Topological semimetal and Fermi-arc surface states in the electronic structure of pyrochlore iridates, *Physical Review B* **83**, 205101 (2011).
- [13] G. Xu, H. Weng, Z. Wang, X. Dai, and Z. Fang, Chern semimetal and the quantized anomalous hall effect in HgCr_2Se_4 , *Phys. Rev. Lett.* **107**, 186806 (2011).
- [14] C. Fang, M. J. Gilbert, X. Dai, and B. A. Bernevig, Multi-Weyl Topological Semimetals Stabilized by Point Group Symmetry, *Physical Review Letters* **108**, 266802 (2012).
- [15] S. M. Young, S. Zaheer, J. C. Y. Teo, C. L. Kane, E. J. Mele, and A. M. Rappe, Dirac Semimetal in Three Dimensions, *Physical Review Letters* **108**, 140405 (2012).
- [16] Z. Wang, Y. Sun, X.-Q. Chen, C. Franchini, G. Xu, H. Weng, X. Dai, and Z. Fang, Dirac semimetal and topological phase transitions in A_3Bi ($\text{A} = \text{Na}, \text{K}, \text{Rb}$), *Physical Review B* **85**, 195320 (2012).
- [17] Z. Wang, H. Weng, Q. Wu, X. Dai, and Z. Fang, Three-dimensional Dirac semimetal and quantum transport in Cd_3As_2 , *Physical Review B* **88**, 125427 (2013).
- [18] B. J. Yang and N. Nagaosa, Classification of stable three-dimensional dirac semimetals with nontrivial topology, *Nat Commun* **5**, 4898 (2014).
- [19] S. A. Yang, H. Pan, and F. Zhang, Dirac and Weyl Superconductors in Three Dimensions, *Physical Review Letters* **113**, 046401 (2014).
- [20] H. Weng, C. Fang, Z. Fang, and X. Dai, Topological semimetals with triply degenerate nodal points in θ -phase tantalum nitride, *Phys. Rev. B* **93**, 241202 (2016).
- [21] H. Weng, C. Fang, Z. Fang, B. A. Bernevig, and X. Dai, Weyl Semimetal Phase in Noncentrosymmetric Transition-Metal Monophosphides, *Physical Review X* **5**, 011029 (2015).
- [22] Z. Zhu, G. W. Winkler, Q. Wu, J. Li, and A. A. Soluyanov, Triple point topological metals, *Phys. Rev. X* **6**, 031003 (2016).
- [23] W. Wu, Z.-M. Yu, X. Zhou, Y. X. Zhao, and S. A. Yang, Higher-order dirac fermions in three dimensions, *Phys. Rev. B* **101**, 205134 (2020).
- [24] H. Weng, Y. Liang, Q. Xu, R. Yu, Z. Fang, X. Dai, and Y. Kawazoe, Topological node-line semimetal in three-dimensional graphene networks, *Physical Review B* **92**, 045108 (2015).
- [25] C. Fang, Y. Chen, H.-Y. Kee, and L. Fu, Topological nodal line semimetals with and without spin-orbital coupling, *Physical Review B* **92**, 081201 (2015).

- [26] Y. Kim, B. J. Wieder, C. L. Kane, and A. M. Rappe, Dirac Line Nodes in Inversion-Symmetric Crystals, *Physical Review Letters* **115**, 036806 (2015).
- [27] R. Yu, H. Weng, Z. Fang, X. Dai, and X. Hu, Topological Node-Line Semimetal and Dirac Semimetal State in Antiperovskite Cu_3PdN , *Physical Review Letters* **115**, 036807 (2015).
- [28] G. Bian, T.-R. Chang, R. Sankar, S.-Y. Xu, H. Zheng, T. Neupert, C.-K. Chiu, S.-M. Huang, G. Chang, I. Belopolski, D. S. Sanchez, M. Neupane, N. Alidoust, C. Liu, B. Wang, C.-C. Lee, H.-T. Jeng, C. Zhang, Z. Yuan, S. Jia, A. Bansil, F. Chou, H. Lin, and M. Z. Hasan, Topological nodal-line fermions in spin-orbit metal PbTaSe_2 , *Nature Communications* **7**, 10556 (2016).
- [29] L.-K. Lim and R. Moessner, Pseudospin vortex ring with a nodal line in three dimensions, *Phys. Rev. Lett.* **118**, 016401 (2017).
- [30] Q. Xu, R. Yu, Z. Fang, X. Dai, and H. Weng, Topological nodal line semimetals in the CaP 3 family of materials, *Physical Review B* **95**, 045136 (2017).
- [31] Q. Wu, A. A. Soluyanov, and T. Bzdusek, Non-abelian band topology in noninteracting metals, *Science* **365**, 1273 (2019).
- [32] Z.-M. Yu, W. Wu, X.-L. Sheng, Y. X. Zhao, and S. A. Yang, Quadratic and cubic nodal lines stabilized by crystalline symmetry, *Phys. Rev. B* **99**, 121106 (2019).
- [33] D. Xiao, M.-C. Chang, and Q. Niu, Berry phase effects on electronic properties, *Reviews of Modern Physics* **82**, 1959 (2010).
- [34] C.-K. Chiu, J. C. Y. Teo, A. P. Schnyder, and S. Ryu, Classification of topological quantum matter with symmetries, *Rev. Mod. Phys.* **88**, 035005 (2016).
- [35] A. P. Schnyder, S. Ryu, A. Furusaki, and A. W. W. Ludwig, Classification of topological insulators and superconductors in three spatial dimensions, *Physical Review B* **78**, 195125 (2008).
- [36] Y. X. Zhao, A. P. Schnyder, and Z. D. Wang, Unified Theory of \mathbb{Z}_2 and $\mathbb{Z}_2\mathbb{Z}_4$ Invariant Topological Metals and Nodal Superconductors, *Physical Review Letters* **116**, 156402 (2016).
- [37] Y. X. Zhao and Y. Lu, \mathcal{PT} -Symmetric Real Dirac Fermions and Semimetals, *Physical Review Letters* **118**, 056401 (2017).
- [38] J. Ahn, D. Kim, Y. Kim, and B.-J. Yang, Band Topology and Linking Structure of Nodal Line Semimetals with \mathbb{Z}_2 Monopole Charges, *Physical Review Letters* **121**, 106403 (2018).
- [39] A. Bouhon, A. M. Black-Schaffer, and R.-J. Slager, Wilson loop approach to fragile topology of split elementary band representations and topological crystalline insulators with time-reversal symmetry, *Physical Review B* **100**, 195135 (2019).
- [40] C. Fang, H. Weng, X. Dai, and Z. Fang, Topological nodal line semimetals, *Chinese Physics B* **25**, 117106 (2016).
- [41] J. Ahn, S. Park, D. Kim, Y. Kim, and B.-J. Yang, Stiefel-Whitney classes and topological phases in band theory, *Chinese Physics B* **28**, 117101 (2019).
- [42] K. Wang, J.-X. Dai, L. B. Shao, S. A. Yang, and Y. X. Zhao, Boundary Criticality of \mathcal{PT} -Invariant Topology and Second-Order Nodal-Line Semimetals, *Physical Review Letters* **125**, 126403 (2020).
- [43] C. Chen, X.-T. Zeng, Z. Chen, Y. X. Zhao, X.-L. Sheng, and S. A. Yang, Second-Order Real Nodal-Line Semimetal in Three-Dimensional Graphdiyne, *Physical Review Letters* **128**, 026405 (2022).
- [44] Z.-M. Yu, W. Wu, Y. X. Zhao, and S. A. Yang, Circumventing the no-go theorem: A single Weyl point without surface Fermi arcs, *Physical Review B* **100**, 041118 (2019).
- [45] W. A. Benalcazar, B. A. Bernevig, and T. L. Hughes, Quantized electric multipole insulators, *Science* **357**, 61 (2017).
- [46] B. Xie, H.-X. Wang, X. Zhang, P. Zhan, J.-H. Jiang, M. Lu, and Y. Chen, Higher-order band topology, *Nature Reviews Physics* **3**, 520 (2021).
- [47] F. Schindler, A. M. Cook, M. G. Vergniory, Z. Wang, S. S. P. Parkin, B. A. Bernevig, and T. Neupert, Higher-order topological insulators, *Science Advances* **4**, eaat0346 (2018).
- [48] A. Bouhon, T. Bzdusek, and R.-J. Slager, Geometric approach to fragile topology beyond symmetry indicators, *Physical Review B* **102**, 115135 (2020).
- [49] Z. Song, Z. Fang, and C. Fang, (d - 2) -Dimensional Edge States of Rotation Symmetry Protected Topological States, *Physical Review Letters* **119**, 246402 (2017).
- [50] J. Langbehn, Y. Peng, L. Trifunovic, F. von Oppen, and P. W. Brouwer, Reflection-Symmetric Second-Order Topological Insulators and Superconductors, *Physical Review Letters* **119**, 246401 (2017).
- [51] F. Schindler, Z. Wang, M. G. Vergniory, A. M. Cook, A. Murani, S. Sengupta, A. Y. Kasumov, R. Deblock, S. Jeon, I. Drozdov, H. Bouchiat, S. Guéron, A. Yazdani, B. A. Bernevig, and T. Neupert, Higher-order topology in bismuth, *Nature Physics* **14**, 918 (2018).
- [52] Q. Wang, C.-C. Liu, Y.-M. Lu, and F. Zhang, High-Temperature Majorana Corner States, *Physical Review Letters* **121**, 186801 (2018).
- [53] C. Fang and L. Fu, New classes of topological crystalline insulators having surface rotation anomaly, *Science Advances* **5**, eaat2374 (2019).
- [54] X.-L. Sheng, C. Chen, H. Liu, Z. Chen, Z.-M. Yu, Y. X. Zhao, and S. A. Yang, Two-Dimensional Second-Order Topological Insulator in Graphdiyne, *Physical Review Letters* **123**, 256402 (2019).
- [55] X. Zhang, T. He, Y. Liu, X. Dai, G. Liu, C. Chen, W. Wu, J. Zhu, and S. A. Yang, Magnetic Real Chern Insulator in 2D Metal-Organic Frameworks, *Nano Letters* **23**, 7358 (2023).
- [56] J. Gong, Y. Wang, Y. Han, Z. Cheng, X. Wang, Z.-M. Yu, and Y. Yao, Hidden Real Topology and Unusual Magnetoelectric Responses in Two-Dimensional Antiferromagnets, *Advanced Materials* **n/a**, 2402232.
- [57] J. Wang, T.-T. Zhang, Q. Zhang, X. Cheng, W. Wang, S. Qian, Z. Cheng, G. Zhang, and X. Wang, 3D Carbon Allotropes: Topological Quantum Materials with Obstructed Atomic Insulating Phases, Multiple Bulk-Boundary Correspondences, and Real Topology, *Advanced Functional Materials* , 2316079 (2024).
- [58] Y. Xu, Z. Song, Z. Wang, H. Weng, and X. Dai, Higher-Order Topology of the Axion Insulator Eu_2As_2 , *Physical Review Letters* **122**, 256402 (2019).
- [59] R. Chen, T. Liu, C. M. Wang, H.-Z. Lu, and X. C. Xie, Field-Tunable One-Sided Higher-Order Topological Hinge States in Dirac Semimetals, *Physical Review Letters* **127**, 066801 (2021).
- [60] E. Lee, R. Kim, J. Ahn, and B.-J. Yang, Two-dimensional higher-order topology in monolayer graphdiyne, *npj*

- Quantum Materials* **5**, 1 (2020).
- [61] H. Xue, Z. Y. Chen, Z. Cheng, J. X. Dai, Y. Long, Y. X. Zhao, and B. Zhang, Stiefel-Whitney topological charges in a three-dimensional acoustic nodal-line crystal, *Nature Communications* **14**, 4563 (2023).
- [62] X. Xiang, Y.-G. Peng, F. Gao, X. Wu, P. Wu, Z. Chen, X. Ni, and X.-F. Zhu, Demonstration of Acoustic Higher-Order Topological Stiefel-Whitney Semimetal, *Physical Review Letters* **132**, 197202 (2024).
- [63] Q. Ma, Z. Pu, L. Ye, J. Lu, X. Huang, M. Ke, H. He, W. Deng, and Z. Liu, Observation of Higher-Order Nodal-Line Semimetal in Phononic Crystals, *Physical Review Letters* **132**, 066601 (2024).
- [64] Y. Zhang, J. Tang, X. Dai, S. Zhang, Z. Cao, and Y. Xiang, Design of a higher-order nodal-line semimetal in a spring-shaped acoustic topological crystal, *Physical Review B* **106**, 184101 (2022).
- [65] X.-L. Du, R. Chen, R. Wang, and D.-H. Xu, Weyl nodes with higher-order topology in an optically driven nodal-line semimetal, *Physical Review B* **105**, L081102 (2022).
- [66] M.-J. Gao, H. Wu, and J.-H. An, Engineering second-order nodal-line semimetals by breaking \mathcal{PT} symmetry and periodic driving, *Physical Review B* **107**, 035128 (2023).
- [67] Y. X. Zhao, Y. Lu, and S. A. Yang, Topological second-order spin-3/2 liquids with hinge Fermi arcs (2020), [arxiv:2005.14500](https://arxiv.org/abs/2005.14500) [cond-mat].
- [68] Y. Li, S. Qian, and C.-C. Liu, Layer Construction of Three-Dimensional Z_2 Monopole Charge Nodal Line Semimetals and prediction of the abundant candidate materials (2023), [arxiv:2309.01566](https://arxiv.org/abs/2309.01566) [cond-mat].
- [69] E. M. W. Janssen and G. A. Wiegers, Phase transitions of gold monobromide, AuBr, *Journal of the Less Common Metals* **57**, P59 (1978).
- [70] E. Janssen and G. Wiegers, Crystal growth and the crystal structures of two modifications of gold monobromide, I-AuBr and P-AuBr, *Journal of the Less Common Metals* **57**, P47 (1978).
- [71] T.-T. Zhang, Z.-M. Yu, W. Guo, D. Shi, G. Zhang, and Y. Yao, From Type-II Triply Degenerate Nodal Points and Three-Band Nodal Rings to Type-II Dirac Points in Centrosymmetric Zirconium Oxide, *The Journal of Physical Chemistry Letters* **8**, 5792 (2017).
- [72] P. M. Lenggenhager, X. Liu, S. S. Tsirkin, T. Neupert, and T. Bzdusek, From triple-point materials to multiband nodal links, *Physical Review B* **103**, L121101 (2021).
- [73] P. M. Lenggenhager, X. Liu, T. Neupert, and T. Bzdusek, Universal higher-order bulk-boundary correspondence of triple nodal points, *Physical Review B* **106**, 085129 (2022).
- [74] P. M. Lenggenhager, X. Liu, T. Neupert, and T. Bzdusek, Triple nodal points characterized by their nodal-line structure in all magnetic space groups, *Physical Review B* **106**, 085128 (2022).
- [75] S. Li, Z. Zhang, X. Feng, W. Wu, Z.-M. Yu, Y. X. Zhao, Y. Yao, and S. A. Yang, Upper bound of a band complex, *Physical Review B* **107**, 235145 (2023).
- [76] H. Xue, Y. Yang, G. Liu, F. Gao, Y. Chong, and B. Zhang, Realization of an Acoustic Third-Order Topological Insulator, *Physical Review Letters* **122**, 244301 (2019).
- [77] X. Zhang, B.-Y. Xie, H.-F. Wang, X. Xu, Y. Tian, J.-H. Jiang, M.-H. Lu, and Y.-F. Chen, Dimensional hierarchy of higher-order topology in three-dimensional sonic crystals, *Nature Communications* **10**, 5331 (2019).
- [78] L. Luo, H.-X. Wang, Z.-K. Lin, B. Jiang, Y. Wu, F. Li, and J.-H. Jiang, Observation of a phononic higher-order Weyl semimetal, *Nature Materials* **20**, 794 (2021).
- [79] Q. Wei, X. Zhang, W. Deng, J. Lu, X. Huang, M. Yan, G. Chen, Z. Liu, and S. Jia, 3D Hinge Transport in Acoustic Higher-Order Topological Insulators, *Physical Review Letters* **127**, 255501 (2021).
- [80] Q. Wei, X. Zhang, W. Deng, J. Lu, X. Huang, M. Yan, G. Chen, Z. Liu, and S. Jia, Higher-order topological semimetal in acoustic crystals, *Nature Materials* **20**, 812 (2021).
- [81] Z. Pu, H. He, L. Luo, Q. Ma, L. Ye, M. Ke, and Z. Liu, Acoustic Higher-Order Weyl Semimetal with Bound Hinge States in the Continuum, *Physical Review Letters* **130**, 116103 (2023).
- [82] Y. Pan, C. Cui, Q. Chen, F. Chen, L. Zhang, Y. Ren, N. Han, W. Li, X. Li, Z.-M. Yu, H. Chen, and Y. Yang, Real higher-order Weyl photonic crystal, *Nature Communications* **14**, 6636 (2023).
- [83] G. Kresse and J. Furthmüller, Efficient iterative schemes for ab initio total-energy calculations using a plane-wave basis set, *Physical Review B* **54**, 11169 (1996).
- [84] G. Kresse and J. Furthmüller, Efficiency of ab-initio total energy calculations for metals and semiconductors using a plane-wave basis set, *Computational Materials Science* **6**, 15 (1996).
- [85] P. E. Blöchl, Projector augmented-wave method, *Physical Review B* **50**, 17953 (1994).
- [86] G. Kresse and D. Joubert, From ultrasoft pseudopotentials to the projector augmented-wave method, *Physical Review B* **59**, 1758 (1999).
- [87] J. P. Perdew, K. Burke, and M. Ernzerhof, Generalized Gradient Approximation Made Simple, *Physical Review Letters* **77**, 3865 (1996).
- [88] J. P. Perdew, K. Burke, and M. Ernzerhof, Perdew, Burke, and Ernzerhof Reply:, *Physical Review Letters* **80**, 891 (1998).
- [89] H. J. Monkhorst and J. D. Pack, Special points for Brillouin-zone integrations, *Physical Review B* **13**, 5188 (1976).
- [90] A. Togo and I. Tanaka, First principles phonon calculations in materials science, *Scripta Materialia* **108**, 1 (2015).
- [91] A. A. Mostofi, J. R. Yates, Y.-S. Lee, I. Souza, D. Vanderbilt, and N. Marzari, Wannier90: A tool for obtaining maximally-localised Wannier functions, *Computer Physics Communications* **178**, 685 (2008).
- [92] A. A. Mostofi, J. R. Yates, G. Pizzi, Y.-S. Lee, I. Souza, D. Vanderbilt, and N. Marzari, An updated version of wannier90: A tool for obtaining maximally-localised Wannier functions, *Computer Physics Communications* **185**, 2309 (2014).
- [93] Q. Wu, S. Zhang, H.-F. Song, M. Troyer, and A. A. Soluyanov, WannierTools: An open-source software package for novel topological materials, *Computer Physics Communications* **224**, 405 (2018).
- [94] J. Taylor, H. Guo, and J. Wang, *Ab Initio* modeling of quantum transport properties of molecular electronic devices, *Physical Review B* **63**, 245407 (2001).